
Aggregating Nested Transformers

Zizhao Zhang¹ Han Zhang² Long Zhao³ Ting Chen² Tomas Pfister¹
¹Google Cloud AI ²Google Research ³Rutgers University

Abstract

Although hierarchical structures are popular in recent vision transformers, they require sophisticated designs and massive datasets to work well. In this work, we explore the idea of nesting basic local transformers on non-overlapping image blocks and aggregating them in a hierarchical manner. We find that the block aggregation function plays a critical role in enabling cross-block non-local information communication. This observation leads us to design a simplified architecture with minor code changes upon the original vision transformer and obtains improved performance compared to existing methods. Our empirical results show that the proposed method NesT converges faster and requires much less training data to achieve good generalization. For example, a NesT with 68M parameters trained on ImageNet for 100/300 epochs achieves 82.3%/83.8% accuracy evaluated on 224×224 image size, outperforming previous methods with up to 57% parameter reduction. Training a NesT with 6M parameters from scratch on CIFAR10 achieves 96% accuracy using a single GPU, setting a new state of the art for vision transformers. Beyond image classification, we extend the key idea to image generation and show NesT leads to a strong decoder that is $8\times$ faster than previous transformer based generators. Furthermore, we also propose a novel method for visually interpreting the learned model. Source code will be released.

1 Introduction

Vision Transformer (ViT) [17] based methods have received much attention recently due to their superior performance on many core visual applications [13, 35]. ViT first splits an input image into patches and patches are treated the same way as tokens in NLP applications. Then several self-attention layers are used to conduct global information communication to extract features for classification. Recent work [13, 17] show ViT models can achieve better accuracy than state-of-the-art convnets [23, 48] when trained on datasets with tens or hundreds of millions of labeled data. However, when trained on smaller datasets, ViT usually underperforms its convnet counterparts. Addressing this data inefficiency is important to make ViT applicable to other application scenarios, e.g., semi-supervised learning [45] and generative modeling [19, 59].

Lack of inductive bias such as locality and translation equivariance is one explanation for the data inefficiency of ViT models. [13] discovers that transformer models learn locality behaviors in a deformable convolution manner [15]: bottom layers attend locally to the surrounding pixels and top layers favor long-range dependency. On the other hand, global self-attention of pixel pairs in high-resolution images is computationally expensive. Reducing the self-attention range can make the model more efficient to train [4]. These type of insights align with the recent methods with local self-attention and hierarchical transformer structures [21, 35, 51]. Instead of holistic global self-attention, these methods perform attention in local image patches. To promote information communication across patches, they propose specialized design such as “haloing operation” [51] and “shifted window” [35]. These variants increase the architecture complexity upon ViT and introduce non-trivial practical implementation. Our work removes these complex architecture designs and focuses on simplification in terms of architecture and training.

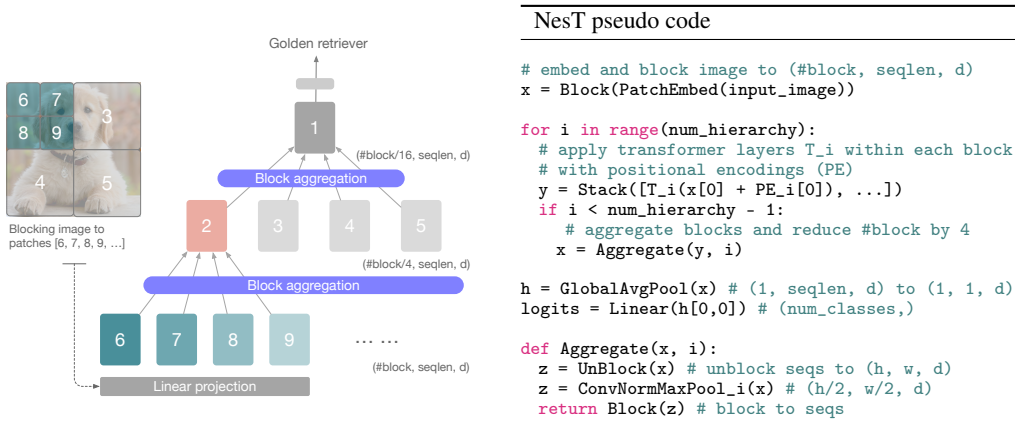


Figure 1: Illustration of NesT with nested transformer hierarchy with pseudo code. Each node T_i processes an image block. The block aggregation is performed between hierarchies ($\text{num_hierarchy}=3$ here) to achieve cross-block communication on the image (feature map) plane.

The proposed NesT simply stacks basic transformer layers to process non-overlapping image blocks individually. Cross-block self-attention is achieved by nesting transformers in a hierarchical manner and connecting them by a proposed aggregation function. Figure 1 illustrates the overall architecture and its simple pseudo code. In summary, this paper makes the following contributions:

- We demonstrate integrating hierarchically nested transformers with the proposed block aggregation function can outperform previous sophisticated (local) self-attention methods, leading to substantially simplified architecture and improved data efficiency.
- The proposed NesT achieves superior ImageNet classification accuracy. For example, training a NesT with 38M/68M parameters attains 83.3%/83.8% ImageNet accuracy on 224×224 image size, outperforming previous methods with up to 57% parameter reduction [35]. The favorable data efficiency of NesT is embodied by its fast convergence, such as achieving 75.9%/82.3% with 30/100 total epoch training. Moreover, NesT achieves matched accuracy on small data benchmarks compared with popular convnets. For example, training a NesT with 6M parameters using a single GPU results in 96% accuracy on CIFAR10, which is the state of the art compared to previous ViT-based methods.
- Beyond classification, we first show that, with proper block de-aggregation, NesT can be repurposed into a strong decoder that achieves better performance than convnets meanwhile has comparable speed, demonstrated by 64×64 ImageNet generation, a critical milestone towards adopting transformers for efficient generative modeling.
- In addition, we propose a novel method to interpret NesT reasoning process by traversing its tree-like structure, providing an unique type of visual interpretability to explain how aggregated local transformers selectively process local visual cues from semantic image patches.

2 The Proposed Method

2.1 Main Architecture

According to Figure 1, our overall design stacks basic transformer layers to conduct local self-attention on every image patch independently and then nest them hierarchically. Coupling of processed information between spatially adjacent blocks is achieved through the proposed block aggregation between every two hierarchies. The overall hierarchy structure can be determined by two key hyper-parameters: patch size $S \times S$ and number of block hierarchies T_d . All blocks inside each hierarchy share one set of parameters.

Given an input of image with shape $H \times W \times 3$, each image patch with size $S \times S$ is linearly projected to a word vector in \mathbb{R}^d . Then all word vectors are partitioned to blocks and flatten to generate input $X \in \mathbb{R}^{b \times T_n \times n \times d}$, where b is the batch size, T_n is the total number of blocks at bottom of the NesT

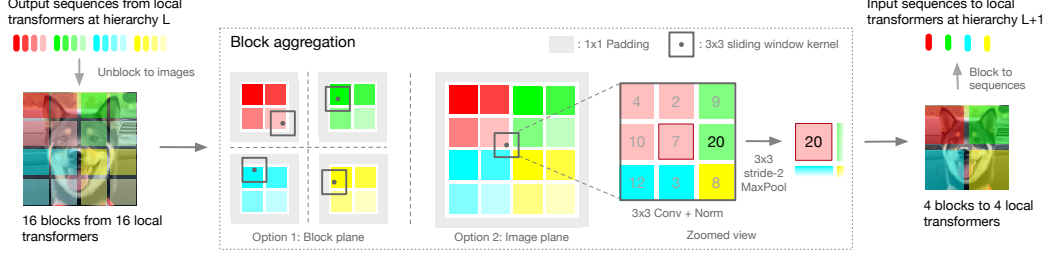


Figure 2: Illustration of block aggregation and comparison when applying that on the block plane versus on the image plane. Although both performing convolution and pooling spatially, performing on the image plane actually allows information communication among blocks (different color palettes) that belong to different merged blocks at the upper hierarchy.

hierarchy, and n is the sequence length (the number of word vectors) inside each block . Note that $T_n \times n = H \times W / S^2$.

Inside each image block, we simply stack a number of basic transformer layers, where each is composed of a multi-head self-attention (MSA) layer followed by a feed-forward fully-connected network (FFN) with skip-connection [23] and LayerNorm (LN) [3]. Trainable positional embedding vectors [49] are added to all sequence vectors in \mathbb{R}^d to encode spatial information before feeding into the block function T :

$$\text{multiple } \times \begin{cases} y = x + \text{MSA}_{\text{NesT}}(x', x', x'), \text{ where } x' = \text{LN}(x) \\ x = y + \text{FFN}(\text{LN}(y)) \end{cases} \quad (1)$$

The FFN is a two-layer network: $\max(0, xW_1 + b)W_2 + b$. Given input $X \in \mathbb{R}^{b \times T_n \times n \times d}$, since all blocks at one NesT hierarchy share parameters, MSA_{NesT} basically applies MSA [52] for all blocks in parallel:

$$\begin{aligned} \text{MSA}_{\text{NesT}}(Q, K, V) &= \text{Stack}(\text{block}_1, \dots, \text{block}_{T_n}), \\ \text{where } \text{block}_i &= \text{MSA}(Q, K, V)W^O. \end{aligned} \quad (2)$$

block_i has shape $b \times n \times d$. Lastly, we simply build a nested hierarchy with a proposed block aggregation - every four spatially connected blocks are merged as one block. The overall design makes NesT straightforward to implement and needs minor code changes based on the original ViT.

2.2 Block Aggregation for Mixing Information Across Blocks

From a high-level view, our NesT leads to hierarchical representations, which shares similarity with several pyramid designs [54, 62]. However, most of the work use global self-attention throughout the layers, interleaved with (spatial) down-sampling. In contrast, we show NesT, which leverages local attention, can lead to much improved data efficiency. In local self-attention, non-local communication is important to maintain translational equivariance [51]. To this end, Halonet [51] allows the query to attend to slightly larger regions than the assigned block. Swin Transformer [35] achieves this by shifting the block partition windows between consecutive self-attention layers to connect adjacent blocks; special masked self-attention is applied to guarantee spatial continuity. However, both have sophisticated designs (with non-trivial implementation) and add extra complexity.

Different from these methods, every block in NesT processes information independently via standard transformer layers, and only communicate and mix global information during block aggregation step via some simple spatial operations (e.g. convolution and pooling). One key ingredient of block aggregation is to perform it in image plane so that information can be exchanged between nearby blocks. The procedure is summarized in Figure 1 and detailed below.

Specifically, the output $X_l \in \mathbb{R}^{b \times \#block \times n \times d}$ at hierarchy l is unblocked to full the image plane $A_l \in \mathbb{R}^{b \times H' \times W' \times d'}$. A number of spatial operations are applied to down-sample feature maps $A'_l \in \mathbb{R}^{b \times H'/2 \times W'/2 \times d'}$. Finally, the feature maps are blocked back to $X_{l+1} \in \mathbb{R}^{b \times \#block/4 \times n \times d'}$ for hierarchy $l+1$. It is easy to see the sequence length n always remains the same and the total number of blocks is reduced by a factor of 4, until reduced to 1 at the top hierarchy (i.e. $\#block/4^{(T_d-1)} = 1$).

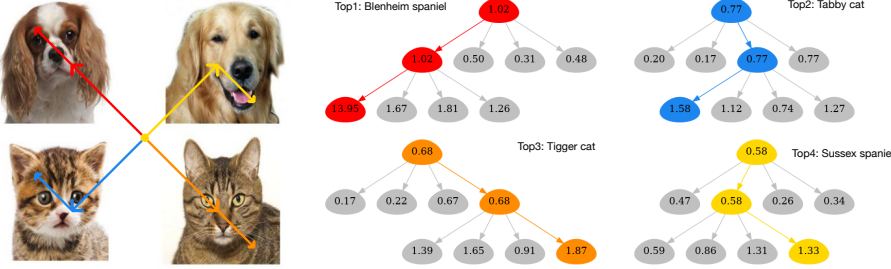


Figure 3: Example results of the proposed GradCAT. Given the left input image (containing four objects), the figure visualizes the top-4 class traversal results (4 colors) using an ImageNet trained NesT (with three tree hierarchies). Each tree node denotes the averaged activation value (i.e. \hat{h}_l defined in Algorithm 1). The traversals can correctly find the model decision path along the tree to locate an image patch belonging to the targeting objects of given target classes.

Therefore, it naturally formats hierarchically nested structure where the “receptive field” expands gradually. $d' \geq d$ depends on the specific model configuration.

Our block aggregation is specially instantiated as a 3×3 convolution followed by LayerNorm and a 3×3 max pooling. Figure 2 explains the core design and the importance of applying it on the image plane (i.e. full image feature maps) versus the block plane (i.e. partial feature maps corresponding to 2×2 blocks that will be merged). The tiny information exchange through the small convolution and max pooling kernels cross block boundaries brings critical gains. We conduct comprehensive experiments to understand the rationale of specific design and verify that block aggregation needs careful design and is also task-aware (see image generation experiments).

3 Generation and Interpretability

3.1 NesT for Image Generation

The data efficiency and simplicity in NesT make it desirable for more complex learning tasks. We repurpose NesT (encoder) into an efficient decoder for generative modeling, and show it has better performance than convnet with comparable speed. Remarkably, it is nearly a magnitude faster than existing transformer based decoders [28].

Creating such a generator is straightforward by “upside-downing” NesT (Table A4 explains architecture details). The input of the model becomes a noise vector and the output is a full-sized image. To support the gradually increased number of blocks, the only modification to NesT is replacing the block aggregation with appropriate block de-aggregation, i.e., un-sampling feature maps (we use pixel shuffle [44]). The feature dimensions in all hierarchies are $(b, nd) \rightarrow (b, 1, n, d) \rightarrow (b, 4, n, d') \dots \rightarrow (b, \#blocks, n, 3)$. The number of blocks increase by a factor of 4. Lastly, we can unblock the output sequence tensor to an image with shape $H \times W \times 3$. The rest adversarial training techniques are based on related methods [19, 59] as explained in experiments. Based on our experiments, it is interesting to find that, similar to our observations in image classification, a carefully-designed block de-aggregation makes the model significantly more effective in performance.

Algorithm 1 Gradient-based class-aware tree traversal (GradGAT).

```

Define:  $A_l$  denotes the feature maps at hierarchy  $l$ .  $Y_c$  is the logit of predicted class  $c$ .  $[\cdot]_{2 \times 2}$  indexes one of  $2 \times 2$  partitions of input maps.
Input:  $\{A_l | l = 2, \dots, T_d\}, \alpha_{T_d} = A_{T_d}, P = []$ 
Output: The traversal path  $P$  from top to bottom
for  $l = [T_d, \dots, 2]$  do
     $h_l = \alpha_l \cdot (-\frac{\partial Y_c}{\alpha_l})$  # obtain targeting activation maps for indexing
     $\hat{h}_l = \text{AvgPool}_{2 \times 2}(h_l) \in \mathbb{R}^{2 \times 2}$  # average activation maps to  $2 \times 2$  partitions, each for a node
     $n_l^* = \arg \max \hat{h}_l, P = P + [n_l^*]$  # find the highest activation value from the  $2 \times 2$  partitions
     $\alpha_l = A_l[n_l^*]_{2 \times 2}$  # index the partition corresponding to the selected node
end for

```

Table 1: Test accuracy on CIFAR with input size 32×32 . Compared convnets are optimized models for CIFAR. All transformer based models are trained from random initialization with the same data augmentation. The number of parameters (millions), GPU memory (MB), and inference throughput (images/s) on single GPU are compared. We minimize the word size $S \times S$ for each transformer based method. DeiT uses $S = 2$. Swin and our NesT uses $S = 1$. * means models tends to diverge.

Arch. base	Method	#Params	GPU	Throughput	C10 (%)	C100 (%)
Convnet	Pyramid-164-48 [20]	1.7M	126M	3715.9	95.97	80.70
	WRN28-10 [57]	36.5M	202M	1510.8	95.83	80.75
Transformer full-attention	DeiT-T [49]	5.3M	158M	1905.3	88.39	67.52
	DeiT-S [49]	21.3M	356M	734.7	92.44	69.78
	DeiT-B [49]	85.1M	873M	233.7	92.41	70.49
	PVT-T [54]	12.8M	266M	1478.1	90.51	69.62
	PVT-S [54]	24.1M	477M	707.2	92.34	69.79
	PVT-B [54]	60.9M	990M	315.1	85.05*	43.78*
Transformer local-attention	CCT-7/3×1 [22]	3.7M	94M	3040.2	94.72	76.67
	Swin-T [35]	27.5M	183M	2399.2	94.46	78.07
	Swin-S [35]	48.8M	311M	1372.5	94.17	77.01
	Swin-B [35]	86.7M	497M	868.3	94.55	78.45
	NesT-T	6.2M	187M	1616.9	96.04	78.69
	NesT-S	23.4M	411M	627.9	96.97	81.70
	NesT-B	90.1M	984M	189.8	97.20	82.56

3.2 Visual Interpretability via Tree Traversal

Differently from existing methods, the nested hierarchy with independent block process in NesT resembles a decision tree that each block is encouraged to learn non-overlapping features and be selected by the block aggregation. This unique behavior motivates us to explore a new method to interpret the model decision making, which is an important topic in convnets [43, 47].

We present a gradient-based class-aware tree-traversal (GradCAT) method (Algorithm 1). The main idea is to find the most valuable traversal from a child node to the root node that contributes to the classification logits the most. Intuitively, at the top hierarchy, each of four child nodes processes one of 2×2 non-overlapping partitions of feature maps A_{T_d} . We can use corresponding activation and class-specific gradient features to trace the high-value information flow recursively from the root to a leaf node. The negative gradient $-\frac{\partial Y_c}{A_l}$ provides the gradient ascent direction to maximize the class c logit, i.e., a higher positive value means higher importance. Figure 3 illustrates an exemplar result.

4 Experiments

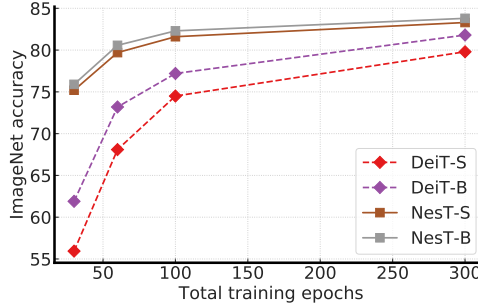
The focus on this work is how to aggregate local transformers and its applicable extensions, so we do not explore the specific per-block configurations (e.g. number of heads and hidden dimensions), which we believe can be optimized through architecture search [48]. We mainly follow previous work [17] to generate three architectures that has comparable capacity (e.g. number of parameters and FLOPS), notated as tiny (NesT-T), small (NesT-S), and base (NesT-B). Most recent ViT based methods follow the training techniques of DeiT [49], which include a mixture of data augmentation like MixUp [58], CutMix [56], RandAugment [14], RandomErasing [64], and regularization like Stochastic Depth [26]. We follow major settings with minor rationale modifications that is we find useful for local self-attention. Appendix A.1 explains all architecture and training details.

4.1 Comparison to Previous State of The Arts

CIFAR We compare to recent methods on CIFAR datasets [32] to investigate data efficiency of different models in Table 1. It is known that previous transformer based methods usually perform poorly on such tasks. All compared methods are trained from random initialization for 300 epochs using 1-2 V100 GPUs, which is a common requirement for convnets. We also list notable convnets that optimized for small images. The methods that work well on large-scale ImageNet does not

Table 2: Comparison on the ImageNet benchmark. The number of parameters (millions), GFLOPS, and inference throughput (images/s) evaluated on a single GPU are also compared. All models are trained from random initialization without extra pre-training.

Arch. base	Method	Size	#Params	GFLOPS	Throughput	Top-1 acc. (%)
Convnet	ResNet-50 [23]	224	25M	3.9G	1226.1	76.2
	RegNetY-4G [40]	224	21M	4.0G	1156.7	80.0
	RegNetY-16G [40]	224	84M	16.0G	334.7	82.9
	EffNet-B3 [48]	300	12M	1.8G	732.1	81.6
	EffNet-B5 [48]	456	30M	9.9G	169.1	83.6
Transformer full-attention	ViT-B/16 [17]	384	86M	55.4G	85.9	77.9
	DeiT-S [49]	224	22M	4.6G	940.4	79.8
	DeiT-B [49]	224	86M	17.5G	292.3	81.8
Transformer local-attention	Swin-T [35]	224	29M	4.5G	755.2	81.3
	Swin-S [35]	224	50M	8.7G	436.9	83.0
	Swin-B [35]	224	88M	15.4G	278.1	83.3
	NesT-T	224	17M	5.8G	633.9	81.5
	NesT-S	224	38M	10.4G	374.5	83.3
	NesT-B	224	68M	17.9G	235.8	83.8



Augmentation Removed	ImageNet Accuracy (%)	
	DeiT-B	NesT-T
None	81.8	81.5
RandomErasing	4.3	81.4
RandAugment	79.6	81.2
CutMix&MixUp	75.8	79.8

Figure 4: Left: Training convergence. NesT achieves better performance than DeiT with the same total epoch of training (each point is a single run). Right: Data augmentation ablations. Results of DeiT-B [49] are reported by its paper. NesT shows less reliance on data augmentation.

necessary work well on small-scale CIFAR. The full self-attention methods are more data hungry. For example, DeiT [49] performs poorly and does not improve given bigger model size. PVT [54] is also a full self-attention design though it has a pyramid structure. PVT-T seems work better than DeiT-T when model size is small, however, the performance largely drops and becomes unstable when scaling up, further suggesting that full self-attention at bottom layers is not desirable for data efficiency. Thus, we do not consider many of this type of co-current work. As discussed in Section 2.2, Swin Transformer [35] shares some high-level ideas with NesT, which we think is the reason that Swin has better accuracy than DeiT and PVT. However, we find it barely improves with increasing model size, suggesting bigger models are more challenging to train with less data. We hypothesize the reasons are two folds: 1) The complex design (i.e. shifted windows with masked MSA) is more data hungry to train. 2) As shown below, the correct design of block aggregation is critical.

NesT improves consistently given bigger model size. Most variants of NesT in Figure 6 outperform compared methods with far better throughput. For example, NesT₃-T ($S = 2$) leads to 94.5% CIFAR10 accuracy with 5384 images/s throughout, 10× faster than Swin-B with 94.6% accuracy.

ImageNet We test NesT on standard ImageNet 2012 benchmarks [16] with commonly used 300 epoch training on TPU in Table 2. The input size is 224×224 and no extra pre-training data is used. DeiT does not use teacher distillation, so it can be viewed as ViT [17] with better data augmentation and regularization. NesT achieves the best performance than compared methods. Especially, NesT-S with 38M parameters matches the 83.3% results of Swin-B, leading to 57% parameter reduction. The strong results of NesT suggest that correctly aggregating local transformer can make the core idea of simple local self-attention work well.

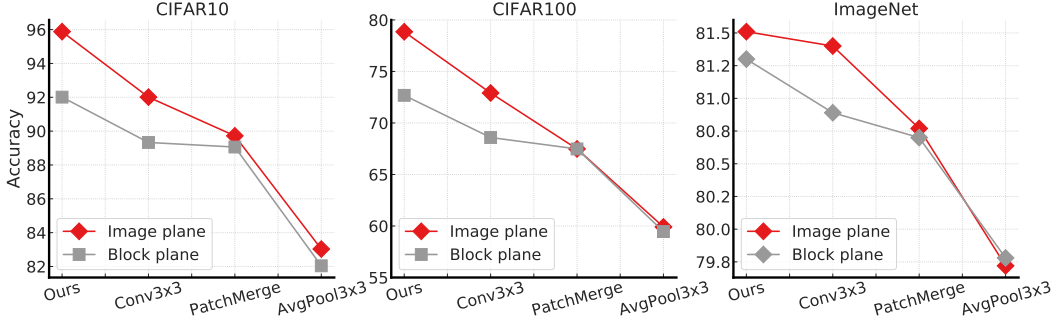


Figure 5: Demonstration of the impact of block aggregation on CIFAR and ImageNet. NesT-T is used. Conv3x3 has stride 2. AvgPool3x3 on ImageNet is followed by Conv1x1 to change hidden dimensions of self-attention. Four plausible block aggregation designs are shown in x-axis, and applied on the image plane and block plane both for comparison. Note that Ours in x-axis is Conv3x3 followed by LayerNorm and MaxPool3x3 (stride 2). More alternatives are validated in Figure A1.

4.2 Training Advantages

We conduct more studies (here and Appendix A.3) to better understand.

Fast convergence. NesT enjoys fairly fast convergence. Figure 4 (left) compares reduced total epoch {30, 60, 100, 300} ImageNet training. The accuracy improvement over DeiT can be up to 14%. NesT-B merely loses 1.5% when reducing the training epoch from 300 to 100. The results suggest that NesT can learn effective visual features much more efficiently than global self-attention methods.

Less sensitivity to data augmentation. NesT uses several kinds of data augmentation following [49]. As shown in Figure 4 (right) and Figure A2, our method shows much higher stability in data augmentation ablation studies compared with DeiT. Data augmentation is critical for global self-attention to generalize, but we think the less dependence on domain or task dependent data augmentation makes an architecture more friendly to other tasks.

4.3 Impact of Block Aggregation

Here we show the design of block aggregation is actually critical for performance and data efficiency while previous related methods neglect. We study from four perspectives to understand the impact: 1) whether unblocking to the full image plane is necessary; 2) how to use convolution; 3) what kinds of pooling to use; 4) whether to perform query down-sampling inside self-attention [51]. Figure 5 and Figure A1 compare the results of different plausible designs to verify these curiosities.

From the results, it is important to find out that: 1) when performing these spatial operations, it is always important to apply on the holistic image plane versus the block plane although both reasonably can introduce spatial priors. 2) small kernel convolution is sufficient and has to be applied ahead of pooling; 3) Max pooling is far better than other options, such as stride-2 sub-sampling and average pooling; 4) sub-sampling the query sequence length (similar to performing sub-sampling on the block plane as illustrated in Figure 2), as used by Halonet [51], performs poorly on data efficient benchmarks. We also experiment PatchMerge from Swin Transformer [35] on both CIFAR and ImageNet. As suggested by the results, our simple block aggregation closes the ImageNet accuracy gap generated by their complex design, suggesting that conceptually negligible difference in aggregating nested transformers can lead to big difference in model performance.

4.4 NesT Hierarchy Variants

We study flexible variants to understand how the hierarchical structure of NesT impacts accuracy. When increasing the hierarchy depth by one, every four blocks are splitted to process four image partitions (see Figure 1). A deeper hierarchy structure makes each block focus on a narrower range of pixel information (i.e., shorter sequence length).

We test combinations with $S = \{1, 2\}$ and depth={2, 3, 4, 5} on NesT-{T, S, B}. Figure 6 compares different variants on two CIFAR datasets. Shallower NesT has clear accuracy drop (although the total

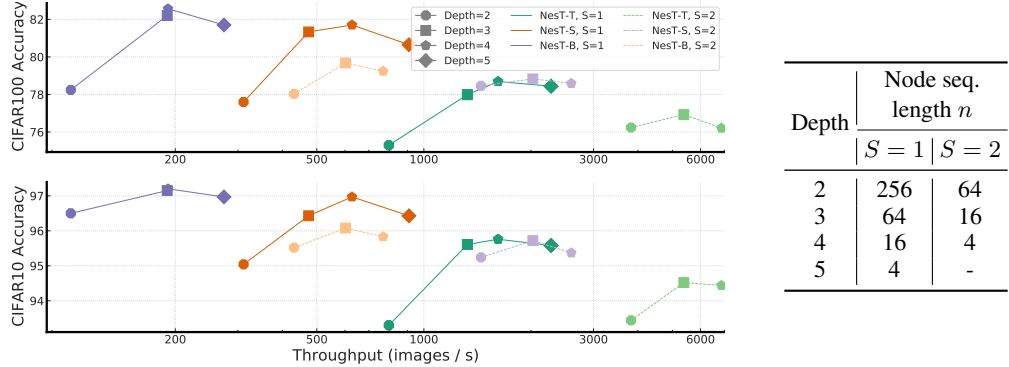


Figure 6: Comparison of NesT hierarchy variants with different depth, word size $S \times S$, and model size. The right table specifies the resulting sequence length given hierarchy depth and S combinations.

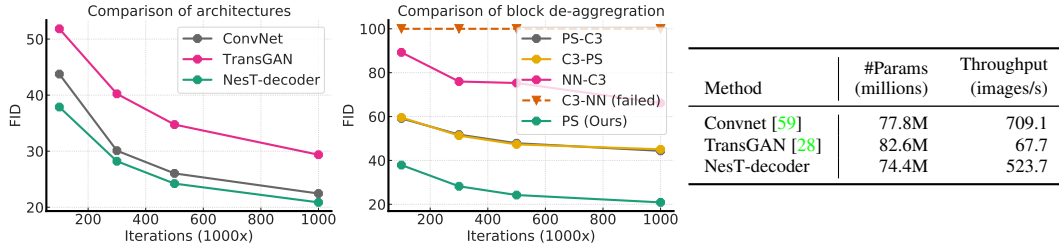


Figure 7: Left: FID comparison for 64×64 ImageNet generation at different training iterations. Middle: FID comparison of different popular un-sampling methods for block de-aggregation, including combinations of pixel shuffling (PS), Conv3x3 (C3), and nearest neighbor (NN). Right: The number of parameters and throughput of compared generators.

number of self-attention layers are the same). It is because, when depth= 1, the model degenerates to a global self-attention method, such as ViT [17]. Depth= 5 has marginal decrease, because the sequence length of all blocks is only $n = 2 \times 2$. Note that we denote NesT₄-B, $S = 1$ as the base NesT with hierarchy depth 4 and word patch size 1×1 . We use the configuration NesT₄, $S = 1$ as the default for the most CIFAR experiments (subscription is omitted sometimes).

4.5 Generative Modeling with NesT as Decoders

We evaluate the generative ability of NesT on ImageNet [42] where all images are resized to 64×64 resolution. We focus on the unconditional image generation setting with the aim to test the effectiveness of different decoders. We compare NesT-decoder to TransGAN [28], a very recent method that uses a full Transformer as the generator, as well as a convnet baseline following the widely-used architecture from [59] (its computationally expensive self-attention module is removed). Results are reported in Figure 7 and Figure A3. NesT-decoder enjoys significantly faster convergence and achieves the best FID and Inception score, importantly, has $8\times$ throughput over TransGAN. More training details are explained in the Appendix A.4.

It is noticeable from Figure 7 (middle) that appropriate un-sampling (or block de-aggregation) impacts the generation quality. Pixel shuffle [44] works the best and the margin is considered surprisingly large compared to other alternatives widely-used in convnets. It aligns with our main findings in classification, suggesting that carelessly injecting spatial operations could make nested local transformers perform undesirably.

4.6 Visual Interpretability

GradGAT results. Figure 8 shows results of the proposed GradGAT. The tree traversal results show that it can locate image blocks from the objects. Each tree node corresponds to a value to reflect the activation strength. The traversal passes the path with the highest strength. The Lighter example is interesting because the ground truth class - lighter/matchstick - actually defines the bottom-right

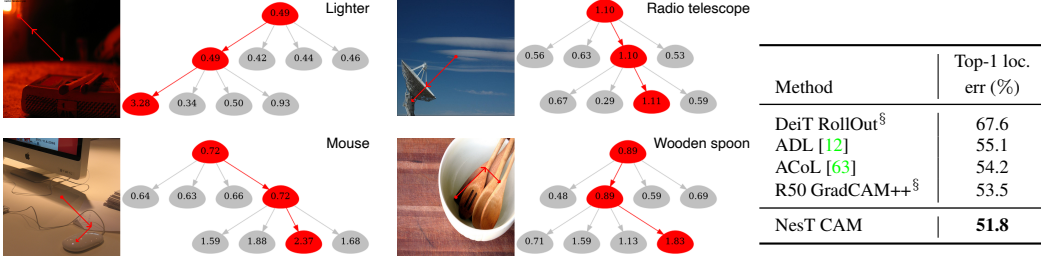


Figure 8: Left: Visualization of the proposed GradGAT. Tree nodes annotate the averaged responses to the predicted class. We use a NesT-S with three tree hierarchies. Right: CAM-based weakly supervised localization comparison on the ImageNet validation set. [§] indicates results obtained by us.

matchstick object while the most salient visual features are actually from the upper-left red light, which conceptually share visual cues with lighter.

Class attention map (CAM) results. NesT does not use class tokens like ViT [17] but a global average pooling before the softmax layer. It gives the advantage to cheaply apply CAM-like [65] method to interpret how well learned representations measure object features without needing any particular algorithms for transformer, such as [7]. In Figure 8 (right), we conduct quantitative evaluation of weakly-supervised object localization, which is a common evaluation protocol for CAM based methods [65]. NesT with basic CAM can even outperform methods specifically for this task. See Figure A4 for qualitative comparison and the Appendix A.5 for comparison details.

Overall, we think decoupling local self-attention (transformer blocks) and global information selection (block aggregation), which is unique our work, has potentials to make models easier to interpret. We leave more explorations as future work.

5 Related Work

Vision transformer based models [13, 17] and self-attention mechanism [41, 51] attract wide interests in recent computer vision community, with explorations of more suitable architectural design that can learn visual representation effectively, such as injecting convnet elements [33, 46, 55], building local or hierarchical structures [54, 62]. Existing methods focus on design a variety of self-attention modifications [35, 51], inevitably superimposed architectural complexity.

Data efficiency is known challenge. Although original ViT [17] can perform better than CNNs with hundreds of millions image pre-training, such data requirement is challenging to be practical. Data-efficient ViT (DeiT) [49, 50] attempts to address this problem by introducing convnet teacher distillation. Although promising, it increases the supervised training complexity. We find there is still rare work trying to address the model data efficiency issue. Existing reported performance on data efficient benchmarks [10, 22] still far under-perform convnets.

ViT is given high expectation to improve vision tasks beyond image classification, with existing studies on generative modeling [11, 27, 28, 39], video understanding [2, 38], segmentation and detection [30, 34, 53], interpretability [1, 6, 7]. We think a deeper understanding of the data efficiency and training difficulties from the architectural perspective could impact the application of these tasks.

6 Conclusion

This paper shows that, with a wisely designed aggregation function, simply aggregating nested transformers can attain better accuracy, data efficiency, and convergence. Thanks to these advantages, we demonstrate its potentials for wider usage beyond classification, including generative modeling and interpretability. We hope the new concept introduced here - aggregation of nested local transformers - can be generalized beyond images.

Some aspects not covered by this work worth future exploration. 1) Will the local transformer design limit the scaling effectiveness to billions of training data? 2) How much can NesT improve core vision tasks like detection and segmentation?

Acknowledgments

We thank Xiaohua Zhai, Sercan Ö. Arik, Jeremy Kubica, Kihyuk Sohn, and Madeleine Udell for their valuable feedback on this paper.

References

- [1] S. Abnar and W. Zuidema. Quantifying attention flow in transformers. *arXiv preprint arXiv:2005.00928*, 2020. [9](#), [18](#)
- [2] H. Akbari, L. Yuan, R. Qian, W.-H. Chuang, S.-F. Chang, Y. Cui, and B. Gong. Vatt: Transformers for multimodal self-supervised learning from raw video, audio and text. *arXiv preprint arXiv:2104.11178*, 2021. [9](#)
- [3] J. L. Ba, J. R. Kiros, and G. E. Hinton. Layer normalization. *arXiv preprint arXiv:1607.06450*, 2016. [3](#)
- [4] I. Beltagy, M. E. Peters, and A. Cohan. Longformer: The long-document transformer. *arXiv preprint arXiv:2004.05150*, 2020. [1](#)
- [5] A. Chattopadhyay, A. Sarkar, P. Howlader, and V. N. Balasubramanian. Grad-cam++: Generalized gradient-based visual explanations for deep convolutional networks. In *WACV*, 2018. [18](#)
- [6] H. Chefer, S. Gur, and L. Wolf. Generic attention-model explainability for interpreting bi-modal and encoder-decoder transformers. *arXiv preprint arXiv:2103.15679*, 2021. [9](#)
- [7] H. Chefer, S. Gur, and L. Wolf. Transformer interpretability beyond attention visualization. *CVPR*, 2021. [9](#)
- [8] T. Chen, S. Kornblith, M. Norouzi, and G. Hinton. A simple framework for contrastive learning of visual representations. In *ICML*, 2020. [14](#)
- [9] T. Chen, S. Kornblith, K. Swersky, M. Norouzi, and G. Hinton. Big self-supervised models are strong semi-supervised learners. *NeurIPS*, 2020. [14](#)
- [10] Z. Chen, L. Xie, J. Niu, X. Liu, L. Wei, and Q. Tian. Visformer: The vision-friendly transformer. *arXiv preprint arXiv:2104.12533*, 2021. [9](#)
- [11] R. Child, S. Gray, A. Radford, and I. Sutskever. Generating long sequences with sparse transformers. *arXiv preprint arXiv:1904.10509*, 2019. [9](#)
- [12] J. Choe and H. Shim. Attention-based dropout layer for weakly supervised object localization. In *CVPR*, 2019. [9](#)
- [13] J.-B. Cordonnier, A. Loukas, and M. Jaggi. On the relationship between self-attention and convolutional layers. *ICLR*, 2020. [1](#), [9](#)
- [14] E. D. Cubuk, B. Zoph, J. Shlens, and Q. V. Le. Randaugment: Practical automated data augmentation with a reduced search space. In *CVPR Workshops*, 2020. [5](#)
- [15] J. Dai, H. Qi, Y. Xiong, Y. Li, G. Zhang, H. Hu, and Y. Wei. Deformable convolutional networks. In *ICCV*, 2017. [1](#)
- [16] J. Deng, W. Dong, R. Socher, L.-J. Li, K. Li, and L. Fei-Fei. Imagenet: A large-scale hierarchical image database. In *CVPR*, 2009. [6](#)
- [17] A. Dosovitskiy, L. Beyer, A. Kolesnikov, D. Weissenborn, X. Zhai, T. Unterthiner, M. Dehghani, M. Minderer, G. Heigold, S. Gelly, et al. An image is worth 16x16 words: Transformers for image recognition at scale. *ICLR*, 2021. [1](#), [5](#), [6](#), [8](#), [9](#)
- [18] J. Gildenblat. Exploring explainability for vision transformers. 2021. [18](#)
- [19] I. J. Goodfellow, J. Pouget-Abadie, M. Mirza, B. Xu, D. Warde-Farley, S. Ozair, A. Courville, and Y. Bengio. Generative adversarial networks. *NeurIPS*, 2014. [1](#), [4](#)

- [20] D. Han, J. Kim, and J. Kim. Deep pyramidal residual networks. In *CVPR*, 2017. 5
- [21] K. Han, A. Xiao, E. Wu, J. Guo, C. Xu, and Y. Wang. Transformer in transformer. *arXiv preprint arXiv:2103.00112*, 2021. 1
- [22] A. Hassani, S. Walton, N. Shah, A. Abduweili, J. Li, and H. Shi. Escaping the big data paradigm with compact transformers. *arXiv preprint arXiv:2104.05704*, 2021. 5, 9, 14
- [23] K. He, X. Zhang, S. Ren, and J. Sun. Deep residual learning for image recognition. In *CVPR*, 2016. 1, 3, 6, 14, 18
- [24] M. Heusel, H. Ramsauer, T. Unterthiner, B. Nessler, and S. Hochreiter. Gans trained by a two time-scale update rule converge to a local nash equilibrium. In *NeurIPS*, 2017. 17
- [25] E. Hoffer, T. Ben-Nun, I. Hubara, N. Giladi, T. Hoefler, and D. Soudry. Augment your batch: Improving generalization through instance repetition. In *CVPR*, 2020. 14
- [26] G. Huang, Y. Sun, Z. Liu, D. Sedra, and K. Q. Weinberger. Deep networks with stochastic depth. In *ECCV*, 2016. 5
- [27] D. A. Hudson and C. L. Zitnick. Generative adversarial transformers. *arXiv preprint arXiv:2103.01209*, 2021. 9
- [28] Y. Jiang, S. Chang, and Z. Wang. Transgan: Two transformers can make one strong gan. *arXiv preprint arXiv:2102.07074*, 2021. 4, 8, 9
- [29] T. Karras, S. Laine, M. Aittala, J. Hellsten, J. Lehtinen, and T. Aila. Analyzing and improving the image quality of stylegan. In *CVPR*, 2020. 17
- [30] B. Kim, J. Lee, J. Kang, E.-S. Kim, and H. J. Kim. Hotr: End-to-end human-object interaction detection with transformers. *CVPR*, 2021. 9
- [31] D. P. Kingma and J. Ba. Adam: A method for stochastic optimization. In *ICLR*, 2014. 17
- [32] A. Krizhevsky, G. Hinton, et al. Learning multiple layers of features from tiny images. 2009. 5
- [33] Y. Li, K. Zhang, J. Cao, R. Timofte, and L. Van Gool. Localvit: Bringing locality to vision transformers. *arXiv preprint arXiv:2104.05707*, 2021. 9
- [34] J. Liang, N. Homayounfar, W.-C. Ma, Y. Xiong, R. Hu, and R. Urtasun. Polytransform: Deep polygon transformer for instance segmentation. In *CVPR*, 2020. 9
- [35] Z. Liu, Y. Lin, Y. Cao, H. Hu, Y. Wei, Z. Zhang, S. Lin, and B. Guo. Swin transformer: Hierarchical vision transformer using shifted windows. *arXiv preprint arXiv:2103.14030*, 2021. 1, 2, 3, 5, 6, 7, 9, 14, 15
- [36] I. Loshchilov and F. Hutter. Fixing weight decay regularization in adam. 2018. 14
- [37] L. Mescheder, A. Geiger, and S. Nowozin. Which training methods for gans do actually converge? In *ICML*, 2018. 17
- [38] D. Neimark, O. Bar, M. Zohar, and D. Asselmann. Video transformer network. *arXiv preprint arXiv:2102.00719*, 2021. 9
- [39] N. Parmar, A. Vaswani, J. Uszkoreit, L. Kaiser, N. Shazeer, A. Ku, and D. Tran. Image transformer. In *ICML*, 2018. 9
- [40] I. Radosavovic, R. P. Kosaraju, R. Girshick, K. He, and P. Dollár. Designing network design spaces. In *CVPR*, 2020. 6
- [41] P. Ramachandran, N. Parmar, A. Vaswani, I. Bello, A. Levskaya, and J. Shlens. Stand-alone self-attention in vision models. *NeurIPS*, 2019. 9
- [42] O. Russakovsky, J. Deng, H. Su, J. Krause, S. Satheesh, S. Ma, Z. Huang, A. Karpathy, A. Khosla, M. Bernstein, et al. Imagenet large scale visual recognition challenge. *IJCV*, 2015. 8

- [43] R. R. Selvaraju, M. Cogswell, A. Das, R. Vedantam, D. Parikh, and D. Batra. Grad-cam: Visual explanations from deep networks via gradient-based localization. In *ICCV*, 2017. 5, 18
- [44] W. Shi, J. Caballero, F. Huszár, J. Totz, A. P. Aitken, R. Bishop, D. Rueckert, and Z. Wang. Real-time single image and video super-resolution using an efficient sub-pixel convolutional neural network. In *CVPR*, 2016. 4, 8, 17
- [45] K. Sohn, D. Berthelot, C.-L. Li, Z. Zhang, N. Carlini, E. D. Cubuk, A. Kurakin, H. Zhang, and C. Raffel. Fixmatch: Simplifying semi-supervised learning with consistency and confidence. *NeurIPS*, 2020. 1
- [46] A. Srinivas, T.-Y. Lin, N. Parmar, J. Shlens, P. Abbeel, and A. Vaswani. Bottleneck transformers for visual recognition. *arXiv preprint arXiv:2101.11605*, 2021. 9
- [47] M. Sundararajan, A. Taly, and Q. Yan. Axiomatic attribution for deep networks. In *ICML*, 2017. 5
- [48] M. Tan and Q. Le. Efficientnet: Rethinking model scaling for convolutional neural networks. In *ICML*, 2019. 1, 5, 6
- [49] H. Touvron, M. Cord, M. Douze, F. Massa, A. Sablayrolles, and H. Jégou. Training data-efficient image transformers & distillation through attention. *arXiv preprint arXiv:2012.12877*, 2020. 3, 5, 6, 7, 9, 14, 15, 16
- [50] H. Touvron, M. Cord, A. Sablayrolles, G. Synnaeve, and H. Jégou. Going deeper with image transformers. *arXiv preprint arXiv:2103.17239*, 2021. 9
- [51] A. Vaswani, P. Ramachandran, A. Srinivas, N. Parmar, B. Hechtman, and J. Shlens. Scaling local self-attention for parameter efficient visual backbones. *CVPR*, 2021. 1, 3, 7, 9, 15
- [52] A. Vaswani, N. Shazeer, N. Parmar, J. Uszkoreit, L. Jones, A. N. Gomez, L. Kaiser, and I. Polosukhin. Attention is all you need. *NeurIPS*, 2017. 3
- [53] H. Wang, Y. Zhu, H. Adam, A. Yuille, and L.-C. Chen. Max-deeplab: End-to-end panoptic segmentation with mask transformers. *CVPR*, 2021. 9
- [54] W. Wang, E. Xie, X. Li, D.-P. Fan, K. Song, D. Liang, T. Lu, P. Luo, and L. Shao. Pyramid vision transformer: A versatile backbone for dense prediction without convolutions. *arXiv preprint arXiv:2102.12122*, 2021. 3, 5, 6, 9
- [55] L. Yuan, Y. Chen, T. Wang, W. Yu, Y. Shi, Z. Jiang, F. E. Tay, J. Feng, and S. Yan. Tokens-to-token vit: Training vision transformers from scratch on imagenet. *arXiv preprint arXiv:2101.11986*, 2021. 9
- [56] S. Yun, D. Han, S. J. Oh, S. Chun, J. Choe, and Y. Yoo. Cutmix: Regularization strategy to train strong classifiers with localizable features. In *ICCV*, 2019. 5
- [57] S. Zagoruyko and N. Komodakis. Wide residual networks. *BMVC*, 2016. 5
- [58] H. Zhang, M. Cisse, Y. N. Dauphin, and D. Lopez-Paz. mixup: Beyond empirical risk minimization. *ICLR*, 2018. 5
- [59] H. Zhang, I. Goodfellow, D. Metaxas, and A. Odena. Self-attention generative adversarial networks. In *ICML*, 2019. 1, 4, 8
- [60] H. Zhang, J. Y. Koh, J. Baldridge, H. Lee, and Y. Yang. Cross-modal contrastive learning for text-to-image generation. In *CVPR*, 2021. 17
- [61] H. Zhang, Z. Zhang, A. Odena, and H. Lee. Consistency regularization for generative adversarial networks. *ICLR*, 2020. 17
- [62] P. Zhang, X. Dai, J. Yang, B. Xiao, L. Yuan, L. Zhang, and J. Gao. Multi-scale vision longformer: A new vision transformer for high-resolution image encoding. *arXiv preprint arXiv:2103.15358*, 2021. 3, 9

- [63] X. Zhang, Y. Wei, J. Feng, Y. Yang, and T. S. Huang. Adversarial complementary learning for weakly supervised object localization. In *CVPR*, 2018. [9](#)
- [64] Z. Zhong, L. Zheng, G. Kang, S. Li, and Y. Yang. Random erasing data augmentation. In *AAAI*, 2020. [5](#)
- [65] B. Zhou, A. Khosla, A. Lapedriza, A. Oliva, and A. Torralba. Learning deep features for discriminative localization. In *CVPR*, 2016. [9](#), [18](#)

A Appendix

We provide more experimental results to complete the experimental sections of the main paper.

A.1 NesT Architecture and Training Details

Table A1: Architecture details of NesT. In each block, the structure is defined using the protocol $[d, h] \times a, b$, where $[d, h]$ refers to [hidden dimensions, number of heads]; a refers to the number of repeated transformer layers V in Equation 1; b refers to the total number of blocks in that hierarchy. Tiny, Small, and Base models have different setup and they are specified below. Note that once the hierarchy is fixed. The sequence length of all blocks are consistent. Configurations of each block for CIFAR and ImageNet are different.

Input size	Seq. length	NesT Hierarchy (Froward direction is 5 to 1)				
		1	2	3	4	5
		$d = [192, 384, 768]$ and $h = [3, 6, 12]$ for model T, S, and B				
32×32 $S = 1$	8×8	$[d, h] \times 4, 1$	$[d, h] \times 4, 4$	$[d, h] \times 4, 16$	-	-
	4×4	$[d, h] \times 3, 1$	$[d, h] \times 3, 4$	$[d, h] \times 3, 16$	$[d, h] \times 3, 64$	-
	2×2	$[d, h] \times 2, 1$	$[d, h] \times 2, 4$	$[d, h] \times 2, 16$	$[d, h] \times 2, 64$	$[d, h] \times 2, 256$
		$d = [96, 96, 128]$, $h = [3, 6, 12]$, and $k = [8, 20, 20]$ for model T, S, and B				
224×224 $S = 4$	14×14	$[d, h] \times 2, 1$	$[2d, 2h] \times 2, 4$	$[4d, 4h] \times k, 16$	-	-

Architecture configuration. The focus on this paper is how to aggregating nested transformers and its extended usage. We do not focus on the specific per-block hyper-parameters (e.g. number of heads and number of MSA layers). We mainly follow previous work to obtain right architectures that has similar capacity (e.g. number of parameters and throughput).

Recall that the overall hierarchy can be determined by two key hyper-parameters: patch size $S \times S$ and hierarchy depth T_d . Just like how ResNet [23] adapts to small and large input sizes, NesT also has different configuration for small input size and large input size. We follow [35, 49] to configure the number of head, hidden dimensions for the tiny, small and base versions. For 32×32 image size, we follow [49]. Specifically, we setup the same number of repeated MSA_{Nest} per block hierarchy. In each hierarchy, the number of hidden dimensions and the number of heads are the same as well. For 224×224 image size, we follow [35]. Therefore, different hierarchy has a gradually increased number of head, hidden dimensions, and number of repeated MSA_{Nest} layers. Table A1 specifies details.

Data Augmentation. We apply the commonly used data augmentation and regularization techniques as [49]. Repeated augmentation [25] in DeiT is not used. In addition, for ImageNet models, we also add color jittering similar to [8, 9] which seems to reduce dependency on local texture cues and slightly improves generalization ($\sim 0.3\%$ on ImageNet).

Training details. We use a base learning rate 2.5e-6 per device. We use the AdamW optimizer [36] and set the weight decay 0.05. The warm-up epoch is 20. The initial learning rate is linearly scaled by a factor of $total_batch_size/256$. For ImageNet training, the total batch size can be 1024 or 2048 when using distributed training on the TPU hardware. We use $[0.2, 0.3, 0.5]$ stochastic death rates for NesT-T, NesT-S, and NesT-B models, respectively. All transformer layer weights and block aggregation weights are initialized using truncated normal distribution.

We use a 0.1 stochastic depth drop rate for all CIFAR models and the warmup is 5 epoch. The CIFAR results of compared transformer based methods, besides CCT-7/3×1 [22], in Table 1 are trained by us. We train these models using their suggested hyper-parameters and we find it works nearly optimal on CIFAR by searching from a set of learning rate and weight decay combinations.

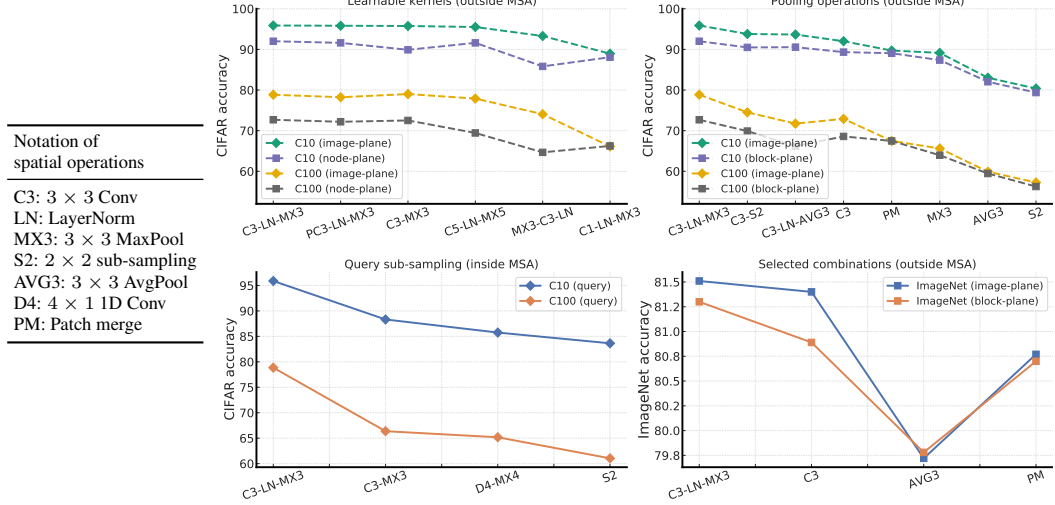


Figure A1: Study the impact of block aggregation on CIFAR and ImageNet. NesT-T is used. We study from different perspectives as explained in the text of the main paper. We verify ImageNet with NesT-T in the bottom-right figure using a subset of representative block aggregation options found on CIFAR datasets. Patch merge [35] and 2×2 sub-sampling [51] are used by previous methods. Since NesT for ImageNet has different hidden dimensions at different hierarchies, AVG3 on ImageNet is followed by a 1×1 convolution to map hidden dimensions. The chosen combinations are specified in x-axis. The leftmost x-axis point (C3-LN-MX3) of each figure is ours.

A.2 Impact of Block Aggregation

Figure A1 shows detailed studies of different block aggregation functions to complete results in Figure 5 of the main paper. Although many of them has tiny difference, it is interesting that the impact to performance is non-trivial. In addition, we find perform query down-sampling inside self attention makes transformers more difficult to train because the skip connection also needs proper down-sampling.

A.3 Ablation Studies

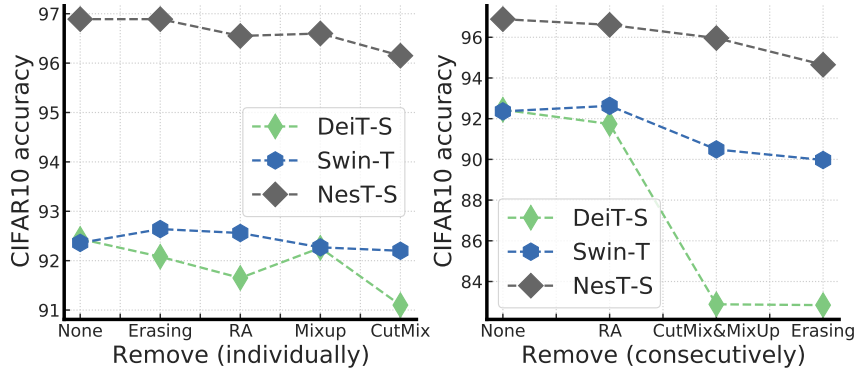


Figure A2: Data augmentation ablation studies on CIFAR10, either removing augmentation individually (middle) or removing (from left to right of x-axis) consecutively (right). None means all are used.

Data augmentation sensitivity. NesT uses several kinds of data augmentation types following DeiT [49]. As shown in Figure A2, our method shows the high stability in augmentation ablation studies compared with DeiT. We speculate the underline reason is that learning effective vision cues is much easier in local attention than in global attention, so Swin Transformer also shows comparable stability. More comparison on ImageNet will be left as future work.

Table A2: Teacher distillation studies on CIFAR datasets. Left: The top two rows of the table are teacher supervised accuracy on CIFAR100. The bottom two rows show accuracy using these trained teachers with standard or strong augmentation. Right: Teacher (PN-164-48 with standard augmentation) distillation effects on DeiT and the proposed NesT. DeiT and NesT are always trained with strong augmentation.

Teacher	Target model	Standard	Strong	Distillation	\times	\checkmark
-	PN-164-48	80.7	81.5			
-	PN-164-270	83.4	84.9			
PN-164-48	NesT-B	84.5	83.7	DeiT-B	92.4	70.5
PN-164-270	NesT-B	84.9	83.8	NesT-B	97.2	82.6
					95.5	81.5
					97.1	84.5

Table A3: Study the impact of number of heads in MSA on the CIFAR10 dataset with NesT₄-B. When #head=96, the hidden dimension used for computing Attention is only 8. However, it can still lead to similar accuracy.

#head in MSA	1	2	3	6	12	24	48	96
Hidden dimension d	768	384	256	128	64	32	16	8
Accuracy	97.1	96.85	96.92	97.07	97.21	97.01	97.03	97.08

Weak teacher distillation. We also explore the teacher distillation proposed by [49], which suggests the inductive bias introduced by convnet teachers are helpful for ViT data efficiency. Table A2 provides detailed distillation study on CIFAR datasets. With such a weak teacher distillation, NesT-B is able to achieve 84.9% CIFAR100 accuracy with 300 epochs and even 86.1% with 1000 epoch training using 2 GPUs.

Convnet teacher distillation [49] is effective to further improve our method as well as DeiT. As explained in [49], the inductive biases of convnets have positive implicit effects to the transformer training. Because data augmentation can improve teacher performance, we question the inductive biases brought by data augmentation is useful or not. Based on our experiments, it seems data augmentation negatively affect the effectiveness of teacher distillation. If the teacher and target model are both trained with strong augmentation, the performance decreases either for a small teacher or a big teacher. In other words, our study suggests that training a high accuracy teacher using strong augmentation negatively impact the distillation effectiveness. Future verification on ImageNet will be left for future work.

Number of heads. We realize different architecture design uses different number of heads for MSA. We attempt to understand the effectiveness of the different configurations. We experiment number of head from 1 to 96 given a fixed $d = 768$ hidden dimension using NesT₄-B. Table A3 shows CIFAR10 results on NesT. It is interesting find the number of heads affects less to the final performance.

A.4 Generative Modeling

Table A4: Architecture details of NesT as image generator. $d = 1024$ and $h = 4$. The input is a reshaped noise vector. At the last hierarchy, there are 64 image blocks. Since the sequence length is 8×8 , it is easy to see that the output image size is 64×64 . At hierarchy 1, the hidden dimension is $1024/64 = 16$. Then a LayerNorm followed by Conv1x1 maps the hidden dimension to the output with shape $64 \times 64 \times 3$.

Input size	Seq. length	NesT Hierarchy (Froward direction is 4 to 1)			
		1	2	3	4
$1 \times n \times d$	8×8	$[d/64, h] \times 2, 64$	$[d/16, h] \times 3, 16$	$[d/4, h] \times 3, 4$	$[d, h] \times 5, 1$

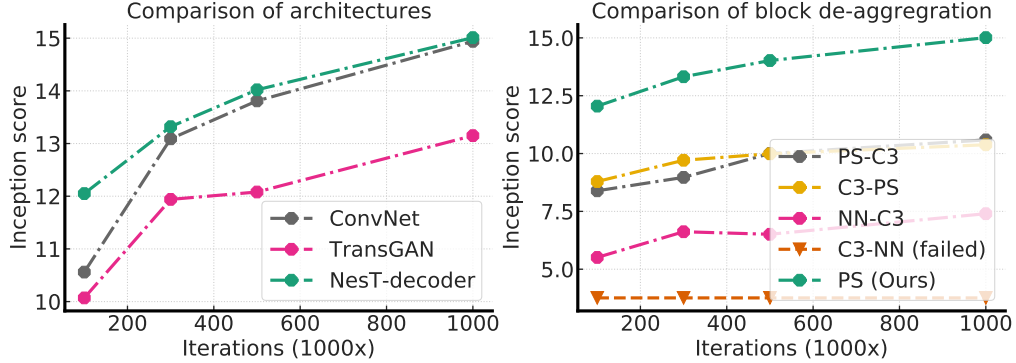


Figure A3: Left: Inception score of 64×64 ImageNet generation of different architectures. Right: Inception score with different un-pooling options. The models used to report the results are the same models in Figure 7 of the main paper.

NesT can become a decoder with minor changes. For fair comparison in terms of model capacity, we configure NesT following the architecture design of TransGAN for image generation. Table A4 specifies the architectural details. The block aggregation layer is swapped to a block de-aggregation layer to achieve the gradually increased image size. Pixel shuffle (PS) [44] is leveraged to increase the image size at block de-aggregation by a factor of two while the hidden dimension is reduced to a quarter of the input.

We adopt the same discriminator architecture as [29] where R1 gradient penalty [37] is applied during training. Adam [31] is utilized for optimization with $\beta_1 = 0$ and $\beta_2 = 0.99$. The learning rate is 0.0001 for both the generator and discriminator with mini-batches of size 256. We use Fréchet Inception Distance (FID) [24] for assessing image quality, which has been shown to be consistent with human judgments of realism [24, 60, 61]. Lower FID values indicate closer distances between synthetic and real data distributions. Figure A3 shows the inception score of different compared methods on 64×64 image generation.

A.5 Interpretability

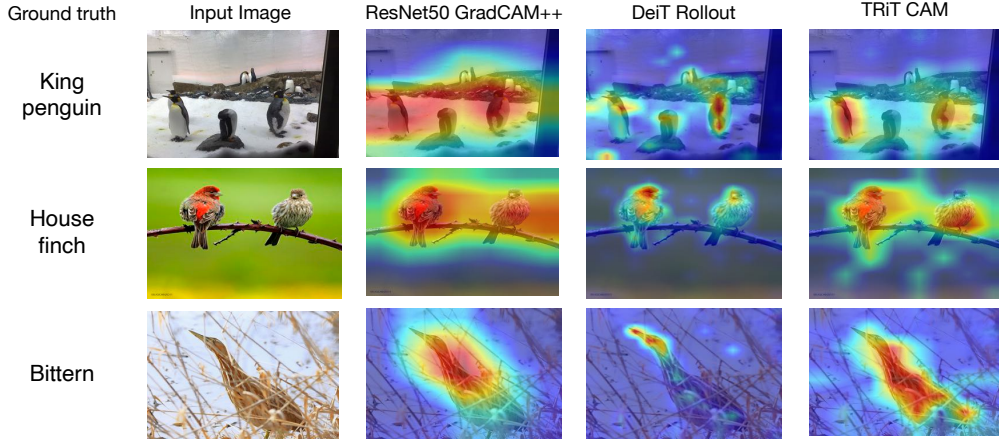


Figure A4: Visualization of CAM based attention results. All models are trained on ImageNet. CAM (vallina) in NesT presents desirable attention results on object regions, including finer attention object converge than DeiT Rollout and less noises than ResNet50 GradCAM++.

GradGAT results. GradGAT always traverses from the root node to one of the leaf node. Since each node of the bottom layer only corresponds to a small non-overlapping patch of the whole image, visualizing GradCAT is less meaningful when the targeting object is large and centered. We find it is true for the majority of ImageNet images although we find our results fairly promising for most

ImageNet images that have small objects. Exploring more comprehensive studies on image datasets with non-centered objects is left for future work.

The proposed GradCAT is partially inspired by how GradCAM [43] in convnets uses gradient information to improve visual attention. Nevertheless, the actual detailed design and serving purposes are distinct.

Class attention map results. Figure A4 compares the qualitative results of CAM, including GradCAM++ [5] with ResNet50 [23], DeiT with Rollout attention [1], and our NesT CAM [65]. We follow [18] to use an improved version of Rollout, which is better than the original version. When converting CAM generated by different methods to bounding boxes, the best threshold of each method varies. We search the best threshold [0, 1] using 0.05 as the interval to find the best number for each method on the ImageNet 50k validation set. It is promising to find that NesT CAM can outperform methods for this task and our baselines. We only use the single forward to obtain bounding boxes.